# Local structure of the superconductor K_{0.8}Fe_{1.6+x}Se_{2}: Evidence of large structural disorder

T. A. Tyson, T. Yu, S. J. Han, M. Croft, G. D. Gu, I. K. Dimitrov, and Q. Li

Phys. Rev. B **85**, 024504 — Published 3 January 2012

DOI: 10.1103/PhysRevB.85.024504

# Local Structure of the Superconductor $K_{0.8}Fe_{1.6+x}Se_2$: Evidence of Large Structural Disorder

T. A. Tyson[1], T. Yu[1], S. J. Han[2], M. Croft[3], G. D. Gu[2], I. K. Dimitrov[2], and Q. Li[2]

[1]Department of Physics, New Jersey Institute of Technology, Newark, NJ 07102, USA

[2]Condensed Matter Physics and Materials Science Department, Brookhaven National Laboratory, Upton NY 11973, USA

[3]Department of Physics and Astronomy, Rutgers University, Piscataway, NJ 08854, USA

## Abstract

The local structure of superconducting single crystals of $K_{0.8}Fe_{1.6+x}Se_2$ with Tc = 32.6 K was studied by x-ray absorption spectroscopy. Near-edge spectra reveal that the average valence of Fe is 2+. The room temperature structure about the Fe, K and Se sites was examined by iron, selenium and potassium K-edge measurements. The structure about the Se and Fe sites shows a high degree of order in the nearest neighbor Fe-Se bonds. On the other hand, the combined Se and K local structure measurements reveal a very high level of structural disorder in the K layers. Temperature dependent measurements at the Fe sites show that the Fe-Se atomic correlation follows that of the Fe-As correlation in the superconductor $LaFeAsO_{0.89}F_{0.11}$ - having the same effective Einstein temperature (stiffness). In $K_{0.8}Fe_{1.6+x}Se_2$, the nearest neighbor Fe-Fe bonds has a lower Einstein temperature and higher structural disorder than in $LaFeAsO_{0.89}F_{0.11}$. The moderate Fe site and high K site structural disorder is consistent with the high normal state resistivity seen in this class of materials. For higher shells, an enhancement of the second nearest neighbor Fe-Fe correlation is found just below Tc possibly due to changes in magnetic or local structural ordering.

PACS: 74.70-b, 78.70.Dm, 61.05.cj

# I. Introduction

The observation of superconductivity in the quaternary ZrCuSiAs-type systems (1111 type) iron arsenide (pnictide) system $LaFeAsO_{1-x}F_x$ [1] created a renaissance in research in superconductivity from both the applied and fundamental physics perspectives. Over the last three years extensive studies have been conducted on the Fe based systems and the results have been reviewed in recent articles (See Ref. [2]). In the $RFeAsO_{1-x}F_x$ (R=rare earth) 1111- type system, optimization of the chemical properties led to the realization of a superconducting transition temperature of ~55 K in $SmFeAsO_{1-\delta}$ [3] , the highest in these new iron systems to date. This first class of materials possesses normal state resistivity values near the transition temperature which are less than 1 mΩ.cm with linear behavior at higher temperatures. Following this, superconductivity was discovered in the system $AFe_2As_2$ system (A=K, Sr, Ba, called the 122 system) [2, 4] with an ambient pressure transition temperature, Tc ~38 K, and resistivity near the transition temperature is ~1 mΩ.cm. Another class of materials referred to as the 111 type (with $CuSb_2$ structure), LiFeAs, was observed to superconduct with a transition near ~18 K [5]. More recently, the PbO type system such as $FeSe_{1-x}$ (with defects on the Fe and Se sites) as well as the Te alloys of this system were found to exhibit superconductivity with Tc near 8 K at ambient temperature for $FeSe_{1-x}$ [6]. Tc was found to be optimized near ~37 K for an external pressure of ~7 GPa [7]. In this system the resistivity values just above the onset of superconductivity are also ~1 mΩ.cm and linear behavior is exhibited above Tc.

Most recently, superconductivity was observed in the system $A_XFe_ySe_2$ (with Tc ~ 31 K in $K_{0.8}Fe_{1.6+x}Se_2$) [8] and has enhanced interest in the field by virtue of the fact the Fe sites possess high ordered magnetic moments and hence the possibility of coexisting antiferromagnetic state and superconducting state is raised. This class of $A_XFe_ySe_2$ (A = alkali or Tl) materials differs from the previous systems in many significant ways. The resistivity just above the transition is > 10 mΩ.cm (more than 10 times higher than that of other iron based systems) and in addition it displays a maximum

in the normal state resistivity vs. temperature curve in the region between ~100 K and 300 K. The magnetic moment on the Fe site is ~3.31 $\mu_B$, the largest of the FeAs and FeSe based systems, and antiferromagnetic order onsets near ~ 550 K. There is evidence for ordered Fe vacancies [9]. $^{57}$Fe Mossbauer spectroscopy measurements indicate that the ordered magnetic state persists below Tc [10]. X-ray diffraction measurements on single crystals suggest an intrinsic phase separation between a majority non-superconducting $\sqrt{5}$ x $\sqrt{5}$ x 1 Fe defect ordered phase and a minority $\sqrt{2}$ x $\sqrt{2}$ x 1 superconducting phase [11].

Understanding the structural changes at the distinct Fe, Se and K ion sites is central to distinguish the important structural components which support superconductivity, when compared with the better characterized $LaFeAsO_{1-x}F_{x.}$ system. Hence, the local structure of superconducting single crystals of $K_{0.8}Fe_{1.6+x}Se_2$ with Tc = 32.6 K was studied by x-ray absorption spectroscopy. Near-edge spectra reveal that the average valence of Fe is 2+. The room temperature structure about the Fe, K and Se sites was examined by iron, selenium and potassium K-edge measurements. The structure about the Se and Fe sites shows a high degree of order in the nearest neighbor Fe-Se bonds. For higher shells, enhancement of the second nearest neighbor Fe-Fe interaction is found just below Tc.

## II. Experimental Methods

High quality single crystal samples of $K_{0.8}Fe_2Se_2$ synthesized by the unidirectional solidification method [12], were extracted 60 to 70 mm from the edge of a 200 mm long crystal bar and were characterized by magnetization and magneto-resistivity measurements. The onset of the transition was at $T_c$ = 32.6 K, with a transition width $\Delta T_c$ = 0.3 K (10%-90%), as seen in Fig. 1(b). X-ray absorption spectra were measured in florescence mode at the National Synchrotron Light Source beamlines X3B (Fe K-edge, 19 K to 300 K), X11A (Se K-edge, room temperature) and X15B (K K-ege, room temperature) at Brookhaven National Laboratory. To reduce the possibility of reaction of the samples with oxygen or moisture, samples were kept in a pure Ar (99.9999%) environment at all times

prior to transferring the samples from the glove box to the experimental x-ray sample chambers. Fe K-Edge measurements were conducted with the sample under vacuum conditions with base pressures < $10^{-6}$ millibar. Measurements at the K K-edge were conducted in a He environment and the Se K-edge measurement was conducted with the sample in a vacuum sealed container. No changes in x-ray spectra were found between successive data scans. Also, no changes were found when comparing data taken at the beginning and end of the complete measurements cycles.

The Se K-edge measurements were conducted with a Lytle type fluorescence detector using an As Z-1 filter (6 absorption lengths) for elastic scatter suppression. The K K-edge spectra were collected with a Si(Li) single element solid state detector and the Fe K-edge data were collected with at 31 Element Ge solid detector using Mn Z-1 Mn filters (9 absorption lengths) for elastic scatter suppression. All data were corrected for self-absorption using the method of Ref. [13]. The measurements were conducted with the single crystal c-axis held ~45° to the incident x-ray beam with the crystal c-axis in the plane of the synchrotron ring. Temperature dependent Fe K-edge measurements were made on warming the single crystal from 19 K on the cold finger of a Displex$^{TM}$ cryostat. The uncertainty in temperature is < 0.25 K. Two to six scans were taken at each temperature. A Fe foil reference was employed for energy calibration at the Fe K-Edge. The reduction of the x-ray absorption fine-structure (XAFS) data was performed using standard procedures [14].

For the fits to the Fe K-edge temperature dependent data, (to treat the distribution on equal footing at all temperatures) the spectra were modeled in R-space by optimizing the integral of the product of the radial distribution functions and theoretical spectra with respect to the measured spectra [15] at each temperature as done in Ref. [16]. Theoretical spectra for atomic shells [17] were derived from the crystal structure data [18]. The predicted trends in the fits and models (Fig. 3) employed the I4/m space group. The Fe K-Edge r-space fits of the Fe-Se and Fe-Fe distribution were confined to the k-range 2.54 < k < 12.8 Å$^{-1}$ and to R-range 1.48 < R < 2.90 Å (with $S_0^2 = 0.73$). Free parameters for each shell in the two shell fits were R (average bond distance) and $\sigma^2$ (the Debye-Waller Factor ($\langle(R - \langle R\rangle)^2\rangle$ mean

squared relative displacement) representing the width of the distribution). The first shell coordination number was held fixed at 4 (Fe-Se bonds) and the second at 3 (Fe-Fe, in plane bonds with Fe1 sites unoccupied (See Ref. [18])). The use of a distribution function approach [15] in place of expansions for the complex XAFS amplitude function enables one to handle broad atomic distributions including the predicted splitting of the Fe-Fe shell into two components with R = 2.69 Å (coordination number =2) and R = 2.92 Å (coordination number =1) for the I4/m structure. For this simple two shell model, the total number of free parameters in each fit was 4, compared to the theoretical maximum number of independent parameters $2\,\Delta k\,\Delta r/\pi + 2 \sim 7$ [19]. Hence, in the temperature dependent fits at Fe K-edge, the coordination numbers were fixed while varying the width and positions of the Gaussian components of the radial distribution functions and the shell positions (R). Errors reported are due to the statistical errors and were based on the spread of parameters over the consecutive scans at fixed temperature. The temperature dependence of the Fe-Se and Fe-Fe Debye-Waller factors ($\sigma^2$) were modeled by a static contribution ($\sigma_0^2$) plus a single parameter ($\theta_E$) Einstein model [20].

In Fig. 3, qualitative model curves were computed for the Fe, Se and K sites with the low symmetry I4/m structure of the $K_{0.8}Fe_{1.6+x}Se_2$ system (see Figure 1(a) and 1(b) and Ref. [18]) using $S_0^2$ = 0.8 and a global $\sigma^2$ values of 0.006 $Å^2$, which are reasonable for room temperature estimates. The simulations using the Feff 7 XAFS simulation code [17] include all shells of atoms out to 6 Å from the absorber sites (Fe, Se or K) and all contribution including multiple scattering signals. For the Se and K sites the weighted average of the simulated spectra (Se1 (20%)/ Se2 (80%) and K1 (20%)/ K2 (80%)) are utilized, while only the Fe2 site is used since all Fe1 sites are considered vacant. In this figure, for the Se K-Edge and the K K-edge the Fourier transforms of the model and data were over the k- ranges $2.63 < k < 17.1$ $Å^{-1}$ and $1.98 < k < 10.0$ $Å^{-1}$, respectively. The Fe K-edge range is given above. Note that the peaks in the Fourier transforms, Figs. 3, 4 and 5(b), are at shorter distances than the corresponding bond distances due to the central atom phase shifts and the scattering atom phase functions. Accurate distances are obtained by model fits.

## III. Results and Discussion

To determine the valence of the sample the near edge spectra or threshold spectra (called x-ray absorption near edge spectrum, XANES) were measured with as step size of 0.2 eV to bring out features in the main line 1s → "4p" peak. The main line spectrum of the superconducting sample is presented as the thick line in Fig. 2(a) and is compared with a group of ~4+, 3+ and 2+ Fe standard compounds. The main-edge energy shows a chemical shift to lower energy with decreasing valence. The chemical shift of the $K_{0.8}Fe_{1.6+x}Se_2$ spectrum falls clearly in the group of Fe 2+ standards. The lack of sharp features of the $K_{0.8}Fe_{1.6+x}Se_2$ spectrum is consistent with broad bands in the Fe-site p-symmetry projected DOS.

The Fe-K pre-edge region, below 7.12 keV, is dominated by 1s transitions into final d-states with the 1s-hole/3d-electron final state Coulomb interaction being what shifts these transitions below the main edge. In Fig. 2(b) the pre-edge spectra for the same set of samples from the previous figure are shown. One can see a systematic chemical shift of the pre-edge features from the "a 2+" to the "b 3+" and finally to the "c ~4+" energy range with increasing Fe valence in the compounds. The $K_{0.8}Fe_{1.6+x}Se_2$ pre-edge clearly falls in the "a 2+" energy range. In general for a 3d transition metals in centrosymmetric local environment the quadrupole allowed 1s to 3d pre-edge transitions increase in intensity with increasing valence. Note that d-p hybridization can, however, enhance the pre-edge feature intensity by introducing stronger dipole allowed transitions. The tetrahedral Fe-Se environment in $K_{0.8}Fe_{1.6+x}Se_2$, and the Fe-S environment in Fe-S-en (en= ethylenediamine) [21], are non-centrosymmetric with d-p hybridization allowed and their pre-edges are both seen to be substantially enhanced in intensity.

In Fig. 1(a), we show the crystal structure of $K_{0.8}Fe_{1.6+x}Se_2$ without defects on the Fe1 and K sites for reference to the structural discussions. The defect structure FeSe layer for two unit cells is shown in Fig. 1(b) with I4/m 4d sites for Fe1 ions vacant . The local structure about the Fe, Se and K sites was examined by room temperature x-ray absorption measurements at the iron K-edge, the selenium

K-edge and the potassium K-edge measurements. In Fig. 3 we show the curves of the measured data and a corresponding model based on the I4/m diffraction model ([18]) as mentioned above. The experimental data are displayed as solid lines and the model curves are displayed as dashed lines.

With respect to the structure about Fe (Fig. 3(a)), the first peak in the Fourier transform (XAFS structure function) has two components from Fe-Se and Fe-Fe (first Fe-Fe correlation) bonds. This peak has two components with the Fe-Fe component being prominent (as a shoulder on the high R side of the main peak) if a high ordered structural model is considered (I4/mmm in Ref. [18(b)]). The first peak in the data is dominated by the Fe-Se pair in the real data due o the weakening of the Fe-Fe contribution due to the interference of the two Fe-Fe components with R = 2.69 Å (coordination number =2) and R = 2.92 Å (coordination number =1) for the I4/m structure. Beyond the first peak there are higher order shells corresponding to the second neighbor Fe-Fe bond, the Fe-K bond and the Fe-Se bond. Analysis of consecutive scans and adjustments of the Fourier transform range to ascertain truncation effects reveal that the weak peaks are the second neighbor Fe-Fe bond, the Fe-K bond and the Fe-Se bonds. However, they are suppressed indicating a high level of disorder in this material. Note that all of these bonds correspond to the same FeSe layer (as in Fig. 1(b)).

With respect to the Se sites one can see in Fig. 3(b) that the first shell about Se is Fe and the second shell would contain K. In Fig. 3(b) we see the structure function for the local structure with respect to the Se sites. The first peak, composed only of Se-Fe bonds, is not a close match with the qualitative model with reduced order. We found that use of the I4/mmm structure gives a better match to the first peak in Fig 3(b). Combined with the results of Fig. 3(a), this suggests that the neither the I4/mmm nor the I4/m models may properly model the local structure of this material. We note that the diffraction models (Ref. [18]) fit the average structure in a unit cell by imposing long range symmetry while in these XAFS measurements no symmetry constraints are added. The results suggest the need for the application of neutron or x-ray pair distribution functions analysis which can combine both long range and local structure solution to create a global view of this system [22] and can make contact with the issue

of phase separation on the nano scale. The second shell about Se corresponds to the Se-K bond and in this region there is negligible amplitude. This indicates a very high level of disorder in the K layers which will be seen in the K K-edge measurements. Near the Se-Se/SeFe shell some non-negligible amplitude is present.

In Fig. 3(c) we see the local structure about the K site compared to the model. Models based on the I4/m (shown here) and the I4/mmm yield the same trend. A very low signal for the structure about K sites is measured. The first neighbor (typically the dominant XAFS signal) is Se, as can be seen from Fig. 1(a). In addition, no signals for higher order peaks such as K-Fe are found. The high level of order of the Se site seen in the Fe K-edge measurements and the absence of the Se-K peak combined with these results at the K K-edge support a model of very high structural disorder of the K sites (potassium layer). More information about the system with respect to the superconducting state and the static disorder in the Fe layer can be obtained from temperature dependent Fe K-edge x-ray measurements.

In Fig. 4, we show the Fourier transform data at the Fe K-edge between 27 K and 31.5 K. The region shown is between 3 Å and 3.7 Å (see Fig. 3(a) and the structural figure in 1(a)) and corresponds mainly to the second neighbor Fe-Fe distance (see Fig. 2) in the same Fe layer. What is observed is that there is an enhancement of the Fe-Fe correlation near 29K, just below the transition to the superconducting state. This enhancement may be due to changes in structural and/or magnetic order near $T_c$ and indicates that more detailed local structural studies, possibly in magnetic fields, may be needed.

We fit the first peak in the temperature dependent data between 19 K and 300 K to determine the behavior of the Fe-Se and Fe-Fe correlations for comparison with the $LaFeAsO_{0.89}F_{0.11}$ superconductor (Fig. 5). Typical consecutive scans at the Fe K-edge are shown in Fig 5(a) and a fit to the first peak (Fe-Se and Fe-Fe shells) is shown in Fig. 5(b) for room temperature data. The temperature dependence of the Fe-Se and Fe-Fe Debye-Waller factors ($\sigma^2$) was modeled by an static disorder contribution ($\sigma_0^2$) plus a

single parameter ($\theta_E$) Einstein model using the functional form $\sigma^2(T) = \sigma_0^2 + \frac{\hbar^2}{2\mu k_B \theta_E} \coth(\frac{\theta_E}{2T})$ [8,23], where $\mu$ is the reduced mass for the bond pair. This simple model represents the bond vibrations as harmonic oscillations of a single effective frequency proportional to $\theta_E$. The parameter $\sigma_0^2$ represents the static disorder. It provides an approach to characterize the relative stiffness of the bonds and can be used to ascertain changes in pair correlations. It differs from the x-ray derived Debye-Waller factor in that the latter describes motion with respect to the equilibrium position of an atom.

The temperature dependence of the $\sigma^2$ for the Fe-Se bond is shown in Fig. 6 (a) and compared with that of the Fe-As bond in $LaFeAsO_{1-x}F_x$ from Ref. [16]. The temperature scale is a log scale to reveal the low temperature region. The $K_{0.8}Fe_{1.6+x}Se_2$ ($\theta_E$ = 308 ± 6 K) and the $LaFeAsO_{0.89}F_{0.11}$ ($\theta_E$ = 316 ± 4 K) systems have the same effective Einstein temperature for the first shell Fe-Se/As bonds within experimental errors. We find that the static disorder ($\sigma_0^2$) parameter for the Fe-Se in $K_{0.8}Fe_{1.6+x}Se_2$ lies closer to the non-superconducting parent compound LaFeAsO than to $LaFeAsO_{0.89}F_{0.11}$. We note also that the effect Einstein temperature of the Fe-Se bond for superconducting phase of the $FeSe_{1-x}Te_x$ system is also of the same value ($\theta_E$ = 300 ± 20 K) [24]. These results indicate that there is similar bonding in the Fe-As-Fe and Fe-Se-Fe networks in these three systems.

With respect to the first neighbor Fe-Fe correlations there are some distinct differences between the $LaFeAsO_{1-x}F_x$ system and the superconducting $K_{0.8}Fe_{1.6+x}Se_2$ material. In Fig. 7 we see that while the first neighbor Fe-Fe correlations in $LaFeAsO_{1-x}F_x$ exhibits negligible (at the level of the data) static disorder, very significant disorder ($\sigma_0^2$ = 0.0038 Å$^2$) exists in the case of the $K_{0.8}Fe_{1.6+x}Se_2$. Moreover, the effective Einstein temperature is significantly lower for this bond than for the x=0.11 $LaFeAsO_{1-x}F_x$ system (244±10 K compared to 304±2 K). The lower Einstein temperature is a direct measurement of the softness of the Fe layer (showing that the Fe layer in $K_{0.8}Fe_{1.6+x}Se_2$ is softened compared to $LaFeAsO_{1-x}F_x$). Compared with the Fe-Se bond, the Fe-Fe first neighbor bond has a significant temperature

dependence over the measured range. These results compared with the enhancement of the second neighbor Fe-Fe correlations near Tc suggest a complex structural and possibly magnetic behavior in this system.

## IV. Summary

Near-edge spectra reveal that the average valence of Fe is 2+. The local structure about the Se and Fe sites shows a high degree of order in the nearest neighbor Fe-Se bonds. On the other hand, the combined Se and K local structure measurements reveal a very high level of structural disorder in the K layers. Temperature dependent measurements at the Fe sites show that the Fe-Se atomic correlation follows that of the Fe-As correlation in the superconductor $LaFeAsO_{0.89}F_{0.11}$ - having the same effective Einstein temperature (stiffness). In $K_{0.8}Fe_{1.6+x}Se_2$, the nearest neighbor Fe-Fe bonds has a lower Einstein temperature and higher structural disorder than in $LaFeAsO_{0.89}F_{0.11}$. The moderate Fe site and high K site structural disorder is consistent with the high normal state resistivity seen in this class of materials. For higher shells, an enhancement of the second nearest neighbor Fe-Fe correlation is found just below Tc and indicate that more detailed local structural studies, possibly in magnetic fields, may be needed.

## V. Acknowledgments

Support for this work was provided by the U.S. Department of Energy, Office of Basic Energy Science, Materials Sciences and Engineering Division under DOE-BES Grant DE-FG02-07ER46402 for T.A.T and T.Y. (NJIT) and under Contract No. DE-AC0298CH10886. DOE Grants (BNL), for S.J.H, G.G, I.K.D, and Q. L. Data acquisition was performed at Brookhaven National Laboratory's National Synchrotron Light Source (NSLS) which is funded by the U. S. Department of Energy.

## Figure Captions

**(Color online) Fig. 1**. (a) Crystal structure of defect free $KFe_2Se_2$ for the I/4m space group. For the superconducting materials it is suggested that random defects occur on the K sites and that the Fe1 sites are unoccupied – resulting in ordered Fe vacancies. (b) View down the c-axis of FeSe layer showing the real structure with vacant Fe1 (I/4m 4d sites) sites for two unit cells. Atom symbols have the same meaning as in panel (a). (c) Resistivity curve for the single crystal samples.

**(Color online) Fig. 2**. Panel (a) shows the K-edge absorption spectrum of superconducting $K_{0.8}Fe_{1.6+x}Se_2$ compared to Fe systems of 2+, 3+ and 4+ valence states. In panel (b) the pre-edge region of the same spectra are also shown. The valence is seen to be strongly 2+ following the behavior of stoichiometric FeS.

**(Color online) Fig.3**. Local structure about the Fe, Se and K sites from the XAFS structure functions in panels (a), (b) and (c) respectively. In each panel, the data are represented by the solid curve and the dashed line a model (I4/m space group) with reasonable thermal/structural parameters. The components of the atomic shells are labeled in each panel.

**(Color online) Fig. 4**. Temperature dependence of the second shell Fe-Fe peak shows enhancement of this second neighbor Fe-Fe shell in the Fe layer near the transition (~30 K). Note that the peaks in the Fourier transforms are at shorter distances than the corresponding bond distances due to the central atom phase shift and the scattering atom phase functions. Accurate distances are obtained by model fits.

**(Color online) Fig. 5.** Two consecutive XAFS scans in k-space, at 300 K are given in (a) and the Fourier transform of the average data is shown with a fit to the Fe-Se and Fe-Fe (first neighbor) peaks in panel (b). The solid line corresponds to the data.

**(Color online) Fig. 6.** Extracted thermal parameters, $\sigma^2(T)$, for the (a) Fe-Se and (b)Fe-As first neighbor bonds in $K_{0.8}Fe_{1.6+x}Se_2$ and $LaFeAsO_{1-x}F_x$ (from Ref. [16]), respectively. The solid lines are with fits to Einstein models. Note the similarity between the two systems with respect to the first shell coordination of Fe.

**(Color online) Fig. 7.** Extracted thermal parameters, $\sigma^2(T)$, for the Fe-Fe second neighbor bonds in $K_{0.8}Fe_{1.6+x}Se_2$ (a) and $LaFeAsO_{1-x}F_x$ (from Ref. [16]) (b), respectively. Compared to the $LaFeAsO_{1-x}F_x$ system [16], $K_{0.8}Fe_{1.6+x}Se_2$ possesses significant static disorder in the Fe layer- consistent with the large normal state resistivity.

**(Color online) Fig. 8.** Extracted Fe-Se (solid circles) and Fe-Fe first neighbor (solid squares) bond distances showing the stronger temperature dependence (smaller Einstein temperature) for the Fe-Fe bond.

**Fig. 1. Tyson *et al.***

**(a)**

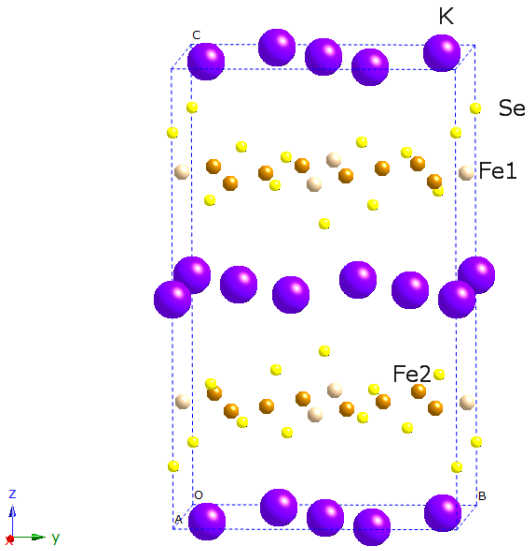


**(b)**

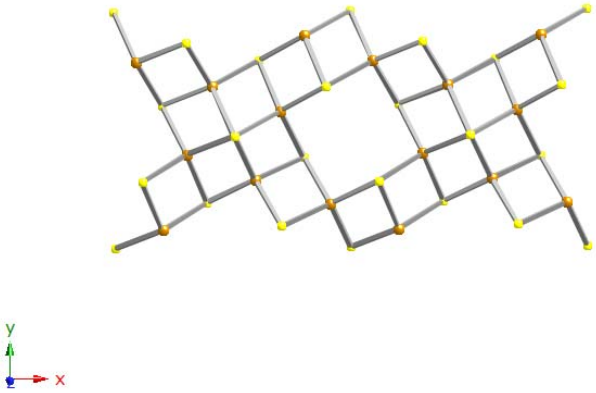


**(c)**

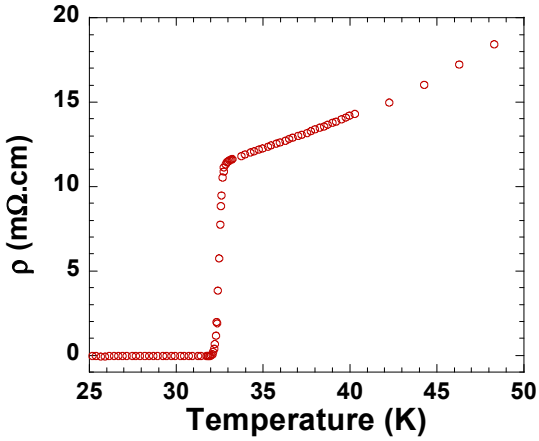

**Fig. 2. Tyson *et al.***

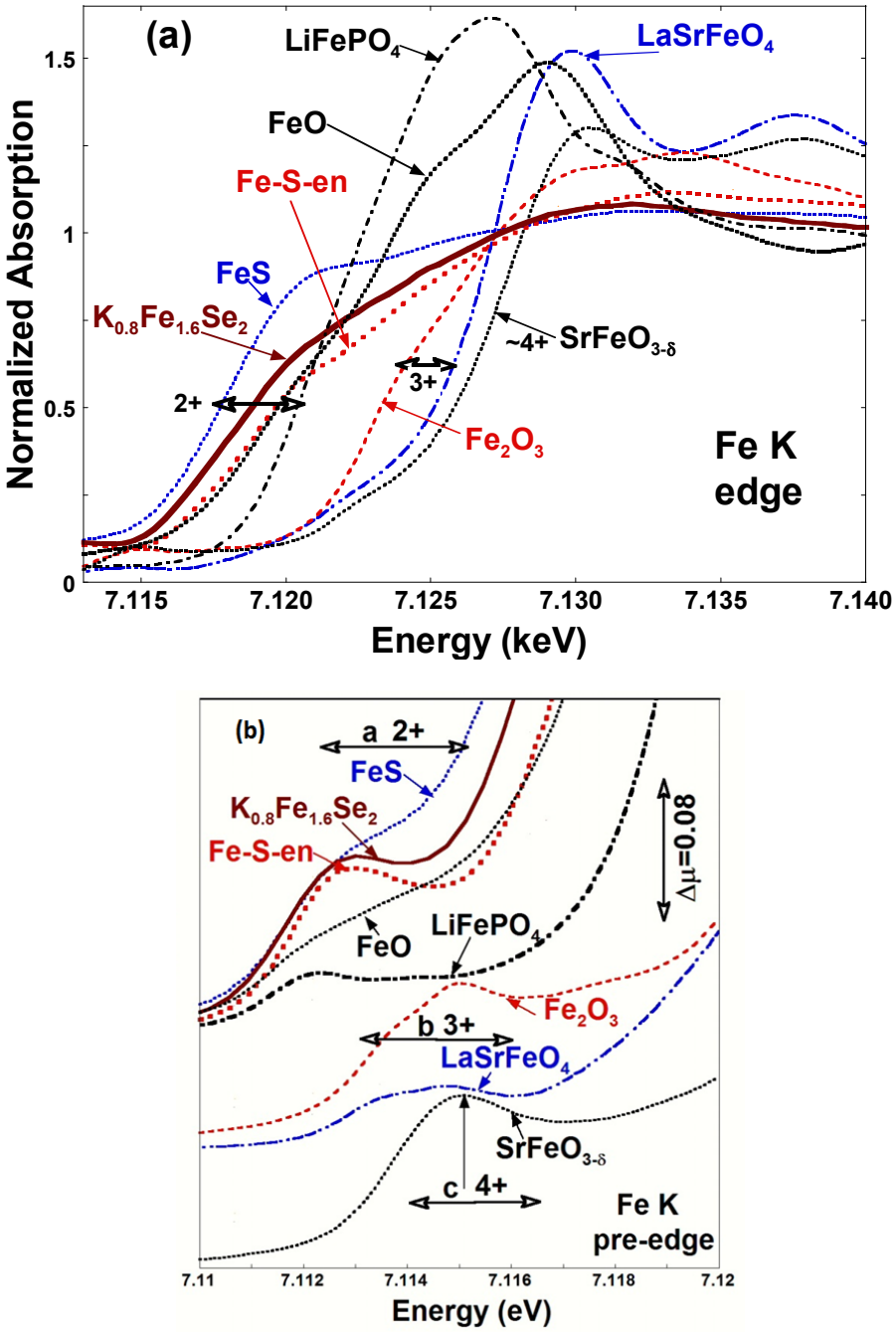

**Fig. 3. Tyson *et al.***

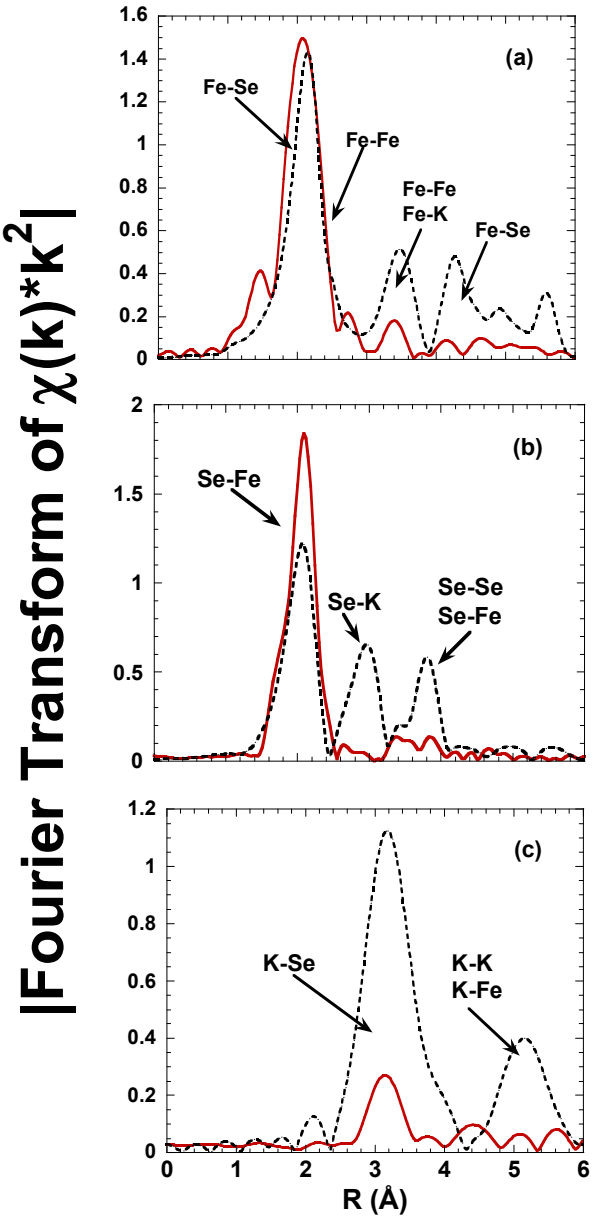


**Fig. 4. Tyson *et al.***

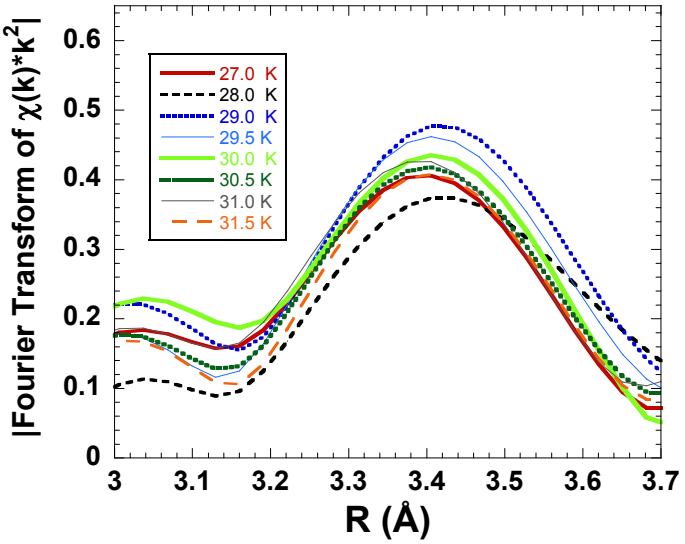
|Fourier Transform of χ(k)*k²|
R (Å)
27.0 K
28.0 K
29.0 K
29.5 K
30.0 K
30.5 K
31.0 K
31.5 K
0
0.1
0.2
0.3
0.4
0.5
0.6
3
3.1
3.2
3.3
3.4
3.5
3.6
3.7

**Fig. 5. Tyson *et al.***

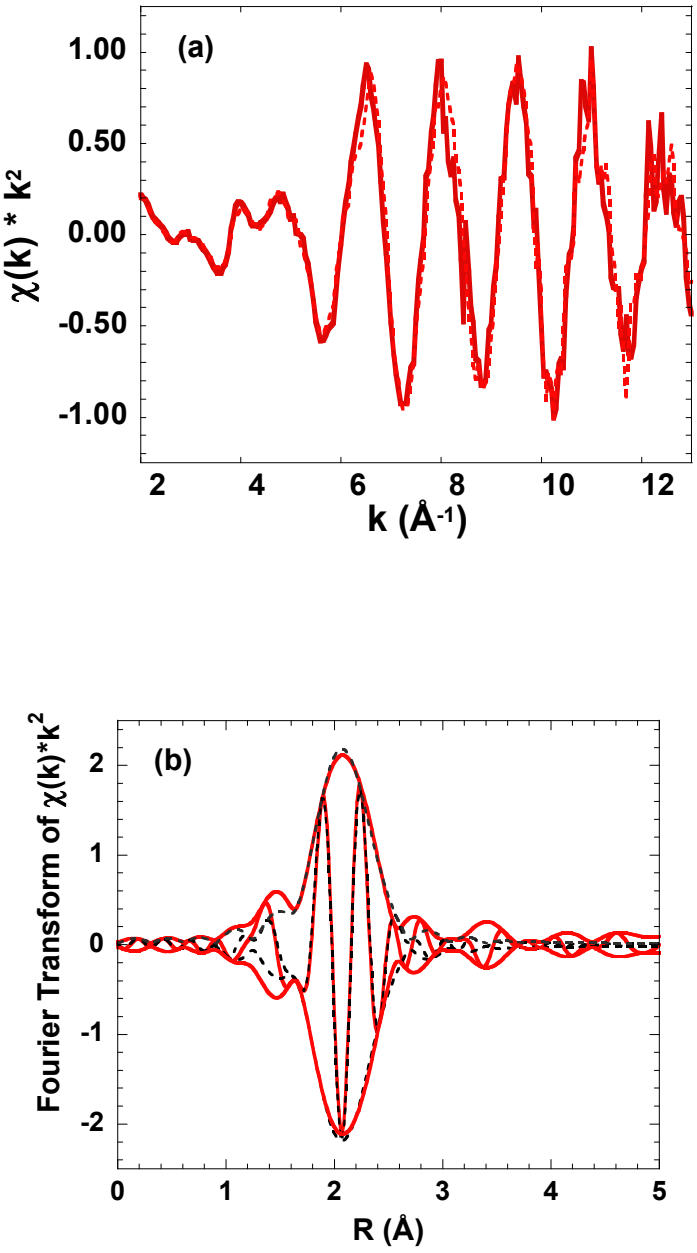

**Fig. 6. Tyson *et al.***

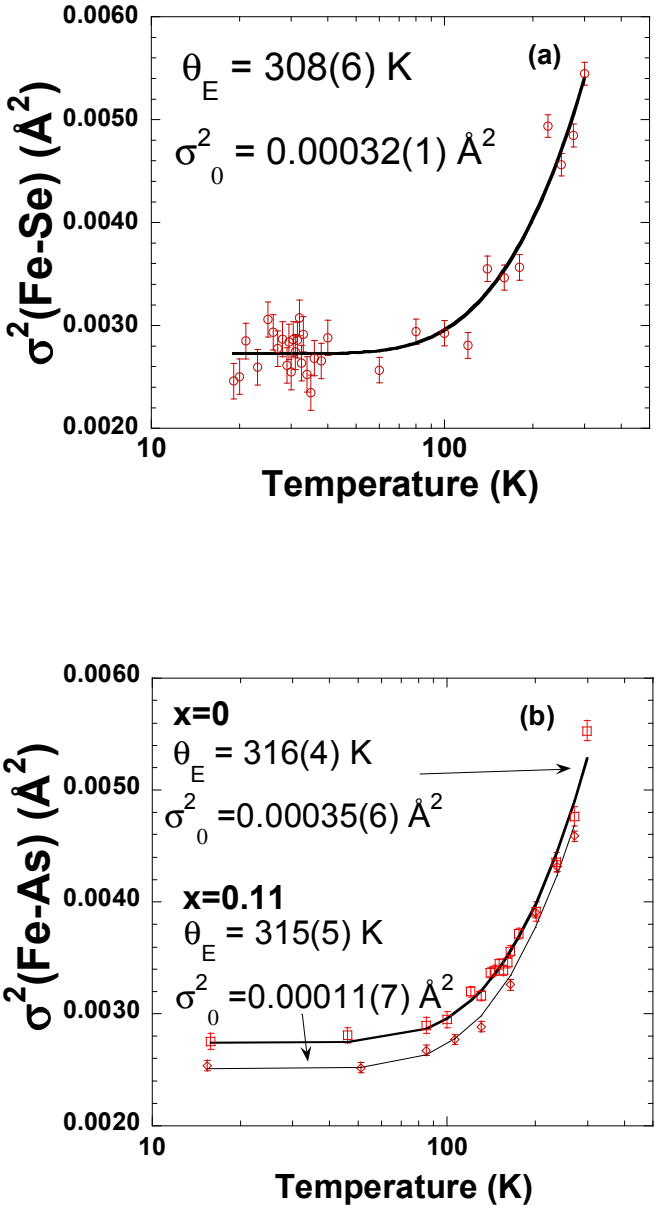

**Fig. 7. Tyson *et al.***

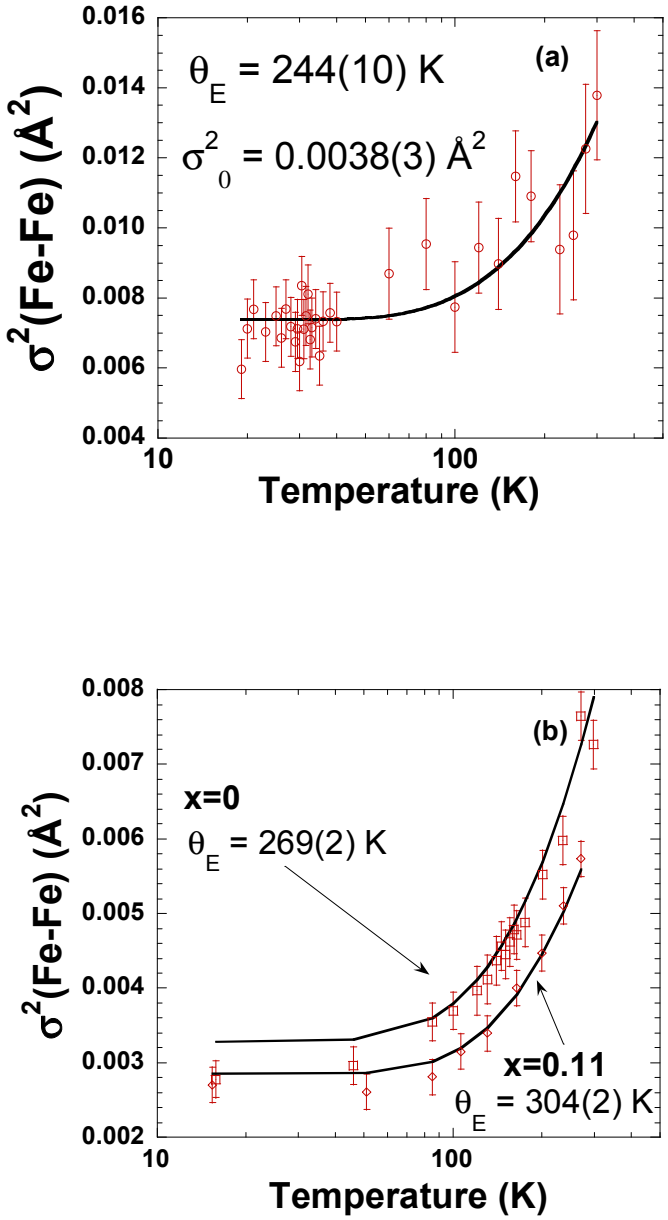

**Fig. 8. Tyson *et al.***

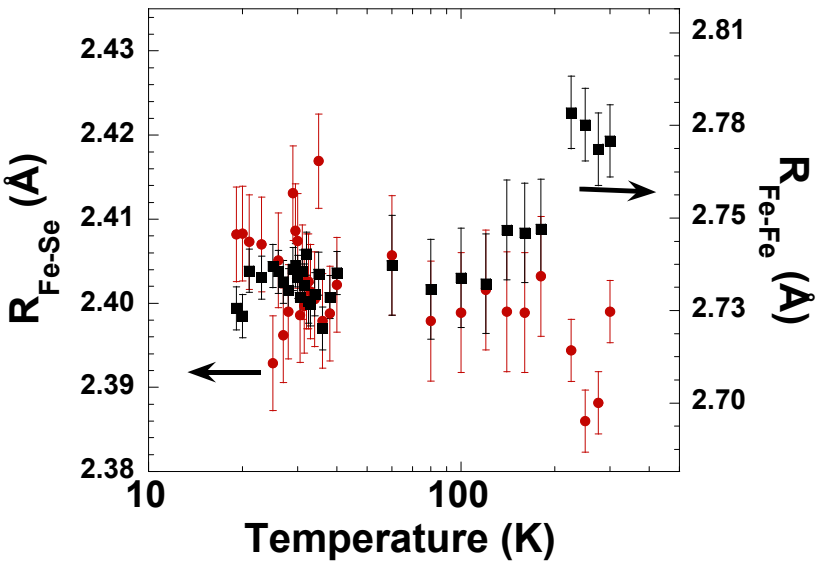

# References


[1] H. Takahashi, K. Igawa, K. Arii, Y. Kamihara, M. Hirano, and H. Hosono, Nature **453**, 376 (2008) and references therein.

[2] (a) H.-H. Wen and S. Li, Annu. Rev. Condens. Matter Phys. **2** , 121 (2011).

(b) J. A. Wilson,J. Phys.: Condens. Matter **22**, 203201/1 (2010).

(c) J. Paglione and R. L. Greene, Nat. Phys. **6** , 645 (2010).

(d) P. M. Aswathy, J. B. Anooja, P. M. Sarun and U. Syamaprasad, Supercond. Sci. Technol. **23**, 073001/1 (2010).

(e) Z.-A. Ren and Z.-X. Zhao, Adv. Mater. (Weinheim, Ger.) **21** , 4584 (2009).

(f) K. Ishida, Y. Nakai and H. Hosono, J. Phys. Soc. Jpn. **78** , 062001/1 (2009).

(g) C. Day, Phys. Today **62** , 36 (2009).

(h) H.-H. Wen, Adv. Mater. (Weinheim, Ger.) **20** , 3764 (2008).

[3] Z.-A. Ren, G.-C. Che, X.-L. Dong, J. Yang, W. Lu, W. Yi, X.-L. Shen, Z.-C. Li, L.-L. Sun, F. Zhou, and Z,-X, Zhao, Euro. Phys. Lett., **83,** 17002 (2008)

[4] M. Rotter, M. Tegel and D. Johrendt, Phys, Rev. Lett, **101**, 107006 (2008).

[5] X. C. Wang, Q. Q. Liu, Y. X. Lv, W. B. Gao, L. X. Yang, R. C. Yu, F. Y. Li and C. Q. Jin, Solid State Commun. **148**, 538 (2008).

[6] F.-C. Hsu, J.-Y. Luo, K.-W. Yeh, T.-K. Chen, T.-W. Huang, P. M. Wu, Y.-C. Lee, Y.-L. Huang, Y.-Y. Chu, D.-C. Yan and M.-K. Wu, Proc. Natl. Acad. Sci. U. S. A. **105** , 14262 (2008).

[7] S. Margadonna, Y. Takabayashi, Y. Ohishi, Y. Mizuguchi, Y. Takano, T. Kagayama, T. Nakagawa, M. Takata and K. Prassides, Phys. Rev. B **80** , 064506 (2009).

[8] J. Gou, S. Jin, G. Wang, K. Zhu, T. Zhou, M. He and X. Chen, Phys. Rev. B **82**, 180520 (2010).

[9](a) P. Zavalij, W. Bao, X. F. Wang, J. J. Ying, X. H. Chen, D. M. Wang, J. B. He, X. Q. Wang, G. F. Chen, P.-Y. Hsieu, Q. Huang and M. A. Green, Phys. Rev. B **83**, 132509 (2011).

(b) W. Bao, Q. Huang, G. F. Chen, M. A. Green, D. M. Wang, J. B. He, X. Q. Wang, and Y. Qiu, Chin. Phys. Lett. **28**, 086104 (2011).

[10] D. H. Ryan, W. N. Rowan-Weetaluktuk, J. M. Cadogan, R. Hu, W. E. Straszheim, S. L. Bud'ko and P. C. Canfield, Phys. Rev. B: Condens. Matter Mater. Phys. **83**, 104526/1 (2011).

[11] (a) A. Ricci, N. Poccia, B. Joseph, G. Arrighetti, L. Barba, J. Plaisier, G. Campi, Y. Mizuguichi, H. Takeya, Y. Takano, N. L. Saini, A. Bianconi, Supercond. Sci. Tech. **24** 082002 (2011).

(b) A. Ricci, N. Poccia, G. Campi, B. Joseph, G. Arrighetti, L. Barba, M. Reynolds, M. Burghammer, H. Takeya, Y. Mizuguichi, , Y. Takano, M. Colapietro, N. L. Saini, A. Bianconi, Phys. Rev B. **84**, 060511(R) (2011).

[12] J. Wen, G. Xu, G. Gu, J. M . Tranquada, and R. J. Birgeneau, Rep. Progress, Physics **74**, 124503 (2011).

[13] C. H. Booth and F. Bridges, Phys. Scr., T **115**, 202 (2005).

[14] B. Ravel and M. Newville, J. Synchrotron Rad. **12**, 537 (2005); *X-Ray Absorption: Principles, Applications, Techniques of EXAFS, SEXAFS and XANES*, edited by D. C. Konningsberger and R. Prins (Wiley, New York, 1988).

[15] K.V. Klementev, Nuclear Instruments and Methods in Physics Research A **448**, 299 (2000).

[16] (a) T. A. Tyson, T. Wu, J. C. Woicik, B. Ravel, A. Ignatov, C. L. Zhang, Z. Qin, T. Zhou and S. W. Cheong, Journal of Applied Physics **108**, 123715 (2010)

(b) T. A. Tyson, T. Wu, J. C. Woicik, B. Ravel, A. Ignatov, C. L. Zhang, Z. Qin, T. Zhou and S. W. Cheong, arXiv:0903.3992 (2009).

[17] A.L. Ankudinov and J.J. Rehr, Phys. Rev. B **56**, R1712 (1997).

[18] (a) P. Zavalij, W. Bao, X. F. Wang, J. J. Ying, X. H. Chen, D. M. Wang, J. B. He, X. Q. Wang, G. F. Chen, P.-Y. Hsieu, Q. Huang and M. A. Green, Phys. Rev. B **83**, 132509 (2011).

(b) J. Guo, X. Chen, G. Wang, T. Zhou, X Lai, S. Jin, S. Wang, and K. Zhu, arXiv:1102.3505 (2011).

[19] E. A. Stern, Phys. Rev. B **48**, 9825 (1993).

[20] J. Mustre de Leon, S. D. Conradson, I. Batistić, A. R. Bishop, I. D. Raistrick, M. C. Aronson, and F. H. Garzon, Phys. Rev. B **45**, 2447 (1992).

[21] M. Wu, J. Rhee, T. J. Emge, H. Yao, J-H Cheng, S. Thiagarajan, M. Croft, R. Yang, and J. Li, Chem. Commun. **46**, 1649–1651 (2010).

[22] T. Egami and S. J. L. Billings, *Underneath the Bragg Peaks: Structural Analysis of Complex Materials* (Pergamon, Amsterdam, 2003).

[23] M. Vaccari and P. Fornasini, J. Syn. Rad. **13**, 321 (2006) and references therein.

[24] B. Joseph, A. Iadecola, A. Purli, L. Simonelli, Y. Mizuguchi, Y. Tanako, N. L. Saini, Phys. Rev. B **82**, 020502(R), (2010).